The Rayleigh Efficiency of Pressure Gain Combustors

Robert J. Blackburn* and Robert J. Miller*
University of Cambridge, Cambridge, U.K.

This paper describes a new method for calculating the performance of pressure gain combustors for gas turbine applications. The method judges the value of a combustor based on the flow's increased potential to do shaft work from combustor inlet to exit. This potential is defined as the work that could be extracted from the flow by a reversible adiabatic turbine exhausting to the combustor supply pressure. A new performance metric, the Rayleigh efficiency, is defined as the increased potential of the flow to do shaft work divided by the heat input. A novel control volume analysis is used, which directly links this performance metric to source terms within the combustor. Two primary source terms are shown: The first is a thermal creation term, which occurs in regions of the flow where combustion heat release occurs at pressures above that of the environment and acts to raise the flow's potential to do shaft work. The term is a nonlinear analog of Lord Rayleigh's acoustic energy creation term, from his 1878 thermoacoustic criterion. The second term is a viscous destruction term that always acts to reduce the flow's potential to do shaft work. In the final part of the paper, the utility of the method is demonstrated using experimental measurements and computational predictions from a SNECMA (Société nationale d'études et de construction de moteurs d'aviation)/ Lockwood-type valveless pulse combustor. The analysis enables a number of previously unanswered questions about pulse combustors to be answered.

Nomenclature

c_p	=	constant-pressure specific heat capacity, J/(kg · K)
c_v	=	constant-volume specific heat capacity, J/(kg · K)
h	=	specific enthalpy, J/kg
m	=	specific system mechanical work potential, J/kg
m_f	=	specific flow mechanical work potential, J/kg
$\dot{M}_D$	=	rate of creation by internal molecular diffusion, J/s
$\dot{M}_{Qi}$	=	rate of creation by internal heat transfer, J/s
$\dot{M}_{Qr}$	=	rate of creation by heat release, J/s
$\dot{M}_{Qs}$	=	rate of addition by heat transfer across surface, J/s
$\dot{M}_W$	=	net rate of work output, J/s
$\dot{M}_\Phi$	=	rate of destruction by viscous dissipation, J/s
$\hat{n}$	=	unit normal vector, out of control volume
p	=	pressure, Pa
$\dot{Q}$	=	heat input rate, J/s
$\dot{q}$	=	volumetric heat input rate, J/(m^3 · s)
q	=	heat flux vector, J/(m^2 · s)
S	=	surface of control volume, m^2
S	=	wall velocity vector, m/s
T	=	temperature, K
$\mathcal{T}$	=	period of combustor cycle, s
t	=	time, s
U	=	flow velocity vector, m/s
V	=	volume of control volume, m^3
v	=	specific volume, m^3/kg
$\dot{W}_x$	=	shaft work output rate, J/s
w_x	=	specific shaft work output, J/kg
γ	=	ratio of specific heat capacities
η_R	=	Rayleigh efficiency
η_{th}	=	thermal efficiency
ϱ	=	density, kg/m^3
$\bar{\bar{\tau}}$	=	viscous stress tensor, N/m^2
τ	=	surface viscous stress vector, equal to $(\bar{\bar{\tau}} \cdot \hat{n})$, N/$m^2$
Φ	=	volumetric rate of viscous dissipation, J/(m^3 · s)

Subscripts

1	=	compressor entry conditions
2	=	compressor exit conditions, combustor entry conditions
2a	=	pressure gain combustor exit conditions
3	=	turbine entry conditions.
4	=	turbine exit conditions
A	=	pressure gain combustor control volume
B	=	combustor and ejector control volume
C	=	gas turbine control volume
D	=	dead-state conditions
IO	=	input/output control volume wall
MW	=	moving control volume wall
se	=	exit of a hypothetical reversible adiabatic turbine exhausting to the dead-state pressure

I. Introduction

A MAJOR obstacle to the development of pressure gain combustors for use in gas turbines is the lack of a consistent metric by which performance can be judged. Pressure gain combustors for direct propulsion applications have an unambiguous metric: thrust-specific fuel consumption [1,2]. By contrast, for gas turbine applications, the choice is ambiguous. Thermal efficiency cannot be used because, for many pressure gain combustors, shaft work out is not their primary objective. Mason et al. [3] proposed the use of a linearized Rayleigh efficiency, defined as the acoustic energy creation term from Lord Rayleigh's thermoacoustic criterion [4] divided by the heat input. This definition has the virtue that the thermal creation term is a direct measure of the creation of acoustic energy (i.e., the underlying pressure gain process). The definition, however, has a number of limitations: 1) the thermal creation term is linear, whereas all practical pressure gain combustors are nonlinear; 2) the definition does not include viscous dissipation inside the combustor and therefore overestimates performance; and 3) some types of pressure gain combustor have shaft work input or output, which is not included in the definition. To solve this problem, this paper proposes the use of a nonlinear form of the Rayleigh efficiency. This new form is defined as the ideal maximum shaft work that can be extracted from the combustor (both through shaft work directly and from the exhaust flow) divided by the heat input [Eq. (1)]. The ideal maximum shaft work that can be extracted from the flow is defined as the work that a reversible adiabatic turbine could extract if it exhausted to the combustor supply pressure. In addition to solving the three limitations highlighted above, this new performance metric
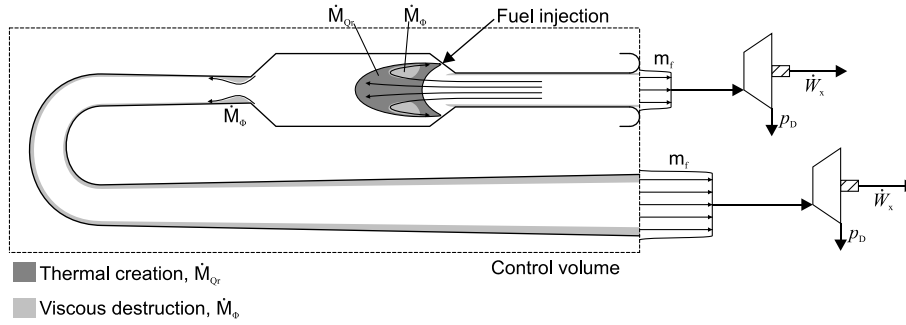
Fig. 1 Creation and destruction of mechanical work potential within a valveless pulse combustor.

will be shown to have the virtue of being easily included in gas turbine cycle analysis.

A second obstacle in the analysis of pressure gain combustors is a lack of a quantitative link between flow phenomena within the combustor, such as regions of heat release or regions of viscous dissipation, and the combustor's overall performance. Miller's recent work in turbomachinery [5] has developed an integral control volume analysis, which directly links the fluid's mechanical work potential, the work which a reversible adiabatic turbine could extract from the flow, with local source terms within the control volume. This analysis shows that two of the main source terms are a thermal creation term (a nonlinear analog of Lord Rayleigh's acoustic energy creation term) and a viscous destruction term. Figure 1 shows a control volume around a SNECMA (Société nationale d'études et de construction de moteurs d'aviation)/Lockwood-type valveless pulse combustor. The figure shows the flux of mechanical work potential m_f of the exit flow and the two source terms within the control volume: the thermal creation term $\dot{M}_{Qr}$ and the viscous destruction term $\dot{M}_\Phi$ (both defined in Sec. II.B).

The paper is made up of three further sections. Section II defines Rayleigh efficiency and develops a control volume analysis that allows the Rayleigh efficiency to be written in terms of the source terms within that control volume. Section III describes a case study of the new analysis technique applied to a valveless pulse combustor. Section IV uses the new control volume analysis to show how the Rayleigh efficiency of a pressure gain combustor can be included in a gas turbine cycle analysis.

The primary aim of Sec. III is a case study demonstrating the new method; however, a number of unanswered questions exist about pulse combustors, which this new method can be used to solve. These include the following: 1) What is the Rayleigh efficiency of a typical valveless pulse combustor? 2) Does the maximum Rayleigh efficiency occur at the minimum specific fuel consumption? 3) Is the combustor's performance limited by the underlying combustion process, not achieving combustion at constant volume, or is the combustion process close to constant volume and the performance limited by high levels of internal dissipation?

II.   Rayleigh Efficiency and Mechanical Work Potential Analysis

In this section, the Rayleigh efficiency is defined and the integral control volume analysis, which links Rayleigh efficiency to source terms, is presented.

A.   The Definition of Rayleigh Efficiency

The Rayleigh efficiency of a control volume is defined as the net shaft work output from the volume, plus the increased potential of the flow to do mechanical work across the volume, divided by the heat input to the volume:

$$\eta_R = \frac{\text{net shaft work out} + \text{net mechanical work potential out}}{\text{heat in}}$$

(1)

Note that the denominator of Eq. (1) represents the actual net heat input rate to the control volume, due to heat release by combustion

and heat transfer over the control volume's boundary, and not the nominal heat input rate based on fuel input.

Rayleigh efficiency is analogous to thermal efficiency, in that it is the ratio of net useful quantities out of a control volume divided by the heat input to the volume. Unlike thermal efficiency, however, Rayleigh efficiency includes the potential of the flow to do mechanical work as a useful quantity. The Rayleigh efficiency of a control volume can be expressed as

$$\eta_R = \frac{\dot{W}_x + \iint_{S_{IO}} \rho \mathsf{m}_f \boldsymbol{U} \cdot \hat{\boldsymbol{n}}\, \mathrm{d}S}{\dot{Q}}$$

(2)

The quantity m_f in Eq. (2), the specific mechanical work potential of the flow, is defined by Miller [5] as

$$\mathsf{m}_f = h - h_{se} + \frac{|\boldsymbol{U}|^2}{2}$$

(3)

Equation (3) represents the specific work that a hypothetical reversible adiabatic turbine could extract from a flow in the presence of a fixed dead-state pressure p_D. It considers only the potential to do mechanical work, while ignoring thermal work potential, the work that a hypothetical reversible Carnot engine could extract from the exhaust of the hypothetical turbine. The surface integral in Eq. (2) represents the net mechanical work potential flux leaving the control volume.

Miller's definition of specific mechanical work potential is illustrated on an enthalpy–entropy chart in Fig. 2. The quantity h_{se} represents the specific enthalpy of the flow at the exit of a reversible adiabatic turbine exhausting to the dead-state pressure. For the case of a perfect gas, specific mechanical work potential can be written as

$$\mathsf{m}_f = c_p T \left(1 - \left(\frac{p_D}{p}\right)^{\frac{\gamma-1}{\gamma}}\right) + \frac{|\boldsymbol{U}|^2}{2}$$

(4)

For any open cycles, exhausting to atmospheric pressure, mechanical work potential is more meaningful than the more familiar concept
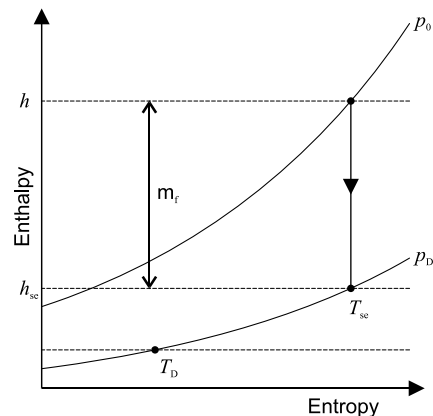

Fig. 2   Enthalpy-entropy diagram showing the definition of mechanical work potential.

of exergy. This is because an exergy analysis assumes that the designer has access to a secondary Carnot cycle with which the exhaust heat can be exploited to increase the work output. In practice, designers of open cycles often do not have access to such a secondary Carnot cycle.

At this point in the paper, the reader may worry that a mechanical work potential analysis is not able to analyze open cycles with waste heat recovery by recuperation. This is because recuperation exploits the exhaust heat to increase work output. However, this exploitation is carried out without the use of a secondary Carnot cycle. It will be shown that mechanical work potential analysis is particularly useful for such cycles. The heat transfer in the recuperator occurs up a finite pressure difference and thus will be shown to result in a source term for mechanical work potential. In such an analysis, a volume integral of this source term, within the recuperator, is proportional to the increase in work output.

It is interesting to note that, for a flow that is nonuniform in space or time, the mass-averaged mechanical work potential is identical to first work-averaging (Cumpsty and Horlock [6]) the flow, and then calculating the mechanical work potential of the uniform flow. This is because both mass-averaging mechanical work potential and work-averaging the flow preserve the potential of the flow to do shaft work.

B. Mechanical Work Potential Balance Equation

In this subsection, the Rayleigh efficiency of a pressure gain combustor is linked to production and destruction terms within the pressure gain combustor control volume. A pressure gain combustor control volume is illustrated in Fig. 1. A mechanical work potential balance equation that links the production of mechanical work potential within a general control volume to fluxes of mechanical work potential into and out of the volume was derived by Miller [5] for perfect gases of uniform composition. It has been extended in this work for nonuniform mixtures of perfect gases. The balance equation is

$$\frac{\mathrm{d}}{\mathrm{d}t}\iiint_V \rho \mathsf{m}\,\mathrm{d}V + \iint_{S_{\mathrm{IO}}} \rho \mathsf{m}_f \boldsymbol{U}\cdot\hat{\boldsymbol{n}}\,\mathrm{d}S$$

$$= \underbrace{-\dot{\mathsf{M}}_W}_{\text{Shaft power out}} + \underbrace{\dot{\mathsf{M}}_{Qs} + \dot{\mathsf{M}}_{Qr}}_{\text{Heat input}} + \underbrace{\dot{\mathsf{M}}_{Qi} - \dot{\mathsf{M}}_\Phi + \dot{\mathsf{M}}_D}_{\text{Internal processes}} \qquad (5)$$

This equation is derived in full in the Appendix.

The two terms on the left side of Eq. (5) represent the storage of mechanical work potential within the control volume and the net flux of mechanical work potential leaving the control volume. The quantity m is simply the specific mechanical work potential of a closed system [5], rather than of a flow, and can be found by subtracting flow work from m_f, as shown in the Appendix. The six terms on the right side represent six mechanisms that add or remove mechanical work potential from the control volume. These six terms are arranged into three groups in Eq. (5), representing the effects of shaft power output from the control volume, heat addition to the control volume, and internal processes within the control volume. The six terms are discussed subsequently.

Net rate of work output:

$$\dot{\mathsf{M}}_W = \iint_{S_{\mathrm{MW}}} ((p - p_D)\boldsymbol{S}\cdot\hat{\boldsymbol{n}} - \boldsymbol{\tau}\cdot\boldsymbol{S})\,\mathrm{d}S \qquad (=\dot{W}_x) \qquad (6)$$

This is the integral of the scalar product of force and velocity over all moving subsurfaces. Hence, it represents the net total shaft power output from the control volume due to either pressure or shear forces.

Rate of addition by heat transfer across surface:

$$\dot{\mathsf{M}}_{Qs} = \oiint\left(1 - \left(\frac{p_D}{p}\right)^{\frac{\gamma-1}{\gamma}}\right)(-\boldsymbol{q})\cdot\hat{\boldsymbol{n}}\,\mathrm{d}S \qquad (7)$$

This is the rate of addition of mechanical work potential to the control volume by heat transfer across the control volume surface.

For a fixed dead-state pressure, its value depends upon the local pressure at which heat is added.

Rate of creation by heat release:

$$\dot{\mathsf{M}}_{Qr} = \iiint_V\left(1 - \left(\frac{p_D}{p}\right)^{\frac{\gamma-1}{\gamma}}\right)\dot{q}\,\mathrm{d}V \qquad (8)$$

This is the rate of creation of mechanical work potential within the control volume by heat release. It is the nonlinear analog of Lord Rayleigh's acoustic thermal creation term [4]. This term represents the key driving mechanism behind pressure gain combustion. Release of heat by combustion at pressures above the dead-state pressure results in the generation of mechanical work potential.

Rate of creation by internal heat transfer:

$$\dot{\mathsf{M}}_{Qi} = \underbrace{\iiint_V\left(\frac{p_D}{p}\right)^{\frac{\gamma-1}{\gamma}}\left(\frac{\gamma-1}{\gamma}\right)\frac{\nabla p}{p}\cdot\boldsymbol{q}\,\mathrm{d}V}_{\text{Heat transfer across }\nabla p}$$

$$+ \underbrace{\iiint_V\left(\frac{p_D}{p}\right)^{\frac{\gamma-1}{\gamma}}\ln\left[\left(\frac{p_D}{p}\right)^{\frac{-1}{\gamma}}\right]\frac{\nabla\gamma}{\gamma}\cdot\boldsymbol{q}\,\mathrm{d}V}_{\text{Heat transfer across }\nabla\gamma} \qquad (9)$$

The first integral represents the creation of mechanical work potential by heat transfer across an internal pressure gradient within the control volume. The second integral represents the creation of mechanical work potential by heat transfer across a gradient of gas composition within the control volume and arises due to the role of the ratio of specific heat capacities in the reversible adiabatic turbine work extraction. It should be noted that exergy destruction by heat transfer across an internal temperature gradient does not necessarily result in the destruction of mechanical work potential. Mechanical work potential is only changed if heat transfer occurs across pressure or composition gradients. It should be noted that Eqs. (7–9) are all of a similar form. In Eqs. (7) and (8) the "value" of the heat addition is given by the Brayton efficiency at which the heat is added. In Eq. (9) the "value" of the heat transfer is given by the gradient of Brayton efficiency across which the heat transfer occurs.

Rate of destruction by viscous dissipation:

$$\dot{\mathsf{M}}_\Phi = \iiint_V\left(\frac{p_D}{p}\right)^{\frac{\gamma-1}{\gamma}}\Phi\,\mathrm{d}V \qquad (10)$$

This is the rate of destruction of mechanical work potential within the control volume by viscous dissipation. For a fixed dead-state pressure, its value depends upon the local pressure at which dissipation occurs. This is due to the well-known reheat effect.

Rate of creation by compositional mixing:

$$\dot{\mathsf{M}}_D = \iiint_V\left(\frac{p_D}{p}\right)^{\frac{\gamma-1}{\gamma}}\ln\left[\left(\frac{p_D}{p}\right)^{\frac{-1}{\gamma}}\right]\frac{1}{\gamma}\frac{\mathrm{D}\gamma}{\mathrm{D}t}\rho c_p T\,\mathrm{d}V \qquad (11)$$

This is the rate of creation of mechanical work potential within the control volume due to compositional mixing. It arises due to the effect of compositional mixing on the ratio of specific heat capacities and thus the ideal work that a reversible adiabatic turbine could extract from the flow.

Pressure gain combustors are necessarily cyclic [7], and the Rayleigh efficiency of a pressure gain combustor can be derived by time-averaging Eq. (5) over the combustor's operating cycle. When this is done, the first term on the left side of Eq. (5) is zero. Moving the shaft power term to the left side and dividing through by the heat input rate gives the expression for the pressure gain combustor's Rayleigh efficiency:
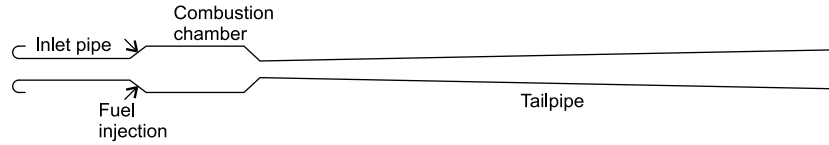
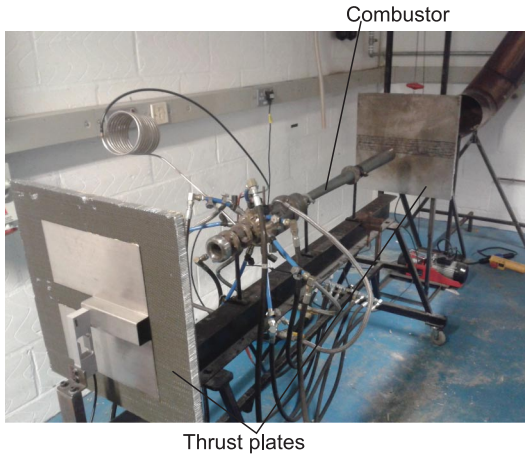**Fig. 3   Valveless pulse combustor schematic.**

Fig. 4   Photograph of the experimental apparatus.

$$\eta_R = \frac{\dot{W}_x + \frac{1}{T}\int_{T}\iint_{S_{IO}} \rho m_f \boldsymbol{U} \cdot \hat{\boldsymbol{n}}\, dS\, dt}{\dot{Q}}$$

$$= \frac{\frac{1}{T}\int_{T}(\dot{M}_{Qs} + \dot{M}_{Qr} + \dot{M}_{Qi} - \dot{M}_{\Phi} + \dot{M}_{D})\, dt}{\dot{Q}} \qquad (12)$$

The left side of Eq. (12) shows the Rayleigh efficiency evaluated on the boundary of the pressure gain combustor control volume. The right side shows the fluid dynamic and thermodynamic processes within the volume that contribute to the Rayleigh efficiency.

The mechanical work potential analysis presented in this section is valid for mixtures of perfect gases. The analysis does not consider chemical reactions. For an exergy analysis, a designer can choose either a thermomechanical exergy analysis (ignoring chemical reactions) or an exact thermomechanical and chemical exergy analysis (considering chemical reactions). In a similar way, an exact thermomechanical and chemical mechanical work potential analysis could be developed. This would be a worthwhile extension of this work. However, in the next section it will be shown that the current method, which ignores chemical reactions, can be used to accurately determine the performance of a pressure gain combustor.

III.   Case Study: Determining the Rayleigh Efficiency of a Valveless Pulse Combustor

In this section, experimental measurements and computational predictions of a valveless pulse combustor are used to demonstrate the mechanical work potential analysis described in Sec. II. First, experimental measurements are used to validate a computational simulation. The results of the simulation are then used to calculate the terms in Eq. (12). The analysis of this section is used to answer the questions stated in the final paragraph of the introduction.

A.   Experimental Methods

Experiments were performed on a valveless SNECMA/Lockwood-type pulse combustor. The particular design geometry was chosen because it had one of the lowest published measurements of specific fuel consumption [8]. The combustor had a total length of 1314 mm and an internal combustion chamber diameter of 75 mm. A schematic of the combustor is shown in Fig. 3. A photograph of the combustor mounted on the experimental rig is shown in Fig. 4.

The combustor was fueled on nonpremixed ethylene. Fuel was injected directly into the combustion chamber, as shown in Fig. 3, through four choked circular orifices.

The fuel massflow rate was determined to a precision error of ± 0.04 g/s. This was achieved by weighing the fuel bottle using precision scales over 30 s periods. The unsteady pressure in the inlet pipe was measured with a Kulite WCTV-312 water-cooled piezo-resistive pressure transducer. The pressure measurement had a precision error of ± 410 Pa. The time-averaged thrusts from the combustor's inlet pipe and tailpipe were measured using thrust plates mounted on Tedea–Huntleigh single-point load cells. The load cells had precisions errors of $\pm 34 \times 10^{-3}$ N. The thrust plate size and location were varied to check independence of measurement to thrust plate configuration.

B.   Numerical Methods

A computational simulation was run using the commercial STAR-CD code. A schematic of the computational domain is shown in Fig. 5. The domain consisted of a combustor and two plenums. The geometry of the combustor matched the internal geometry of the experimental combustor. The walls of the combustor were modeled as adiabatic, no-slip walls. In reality, a pulse combustor has a fairly
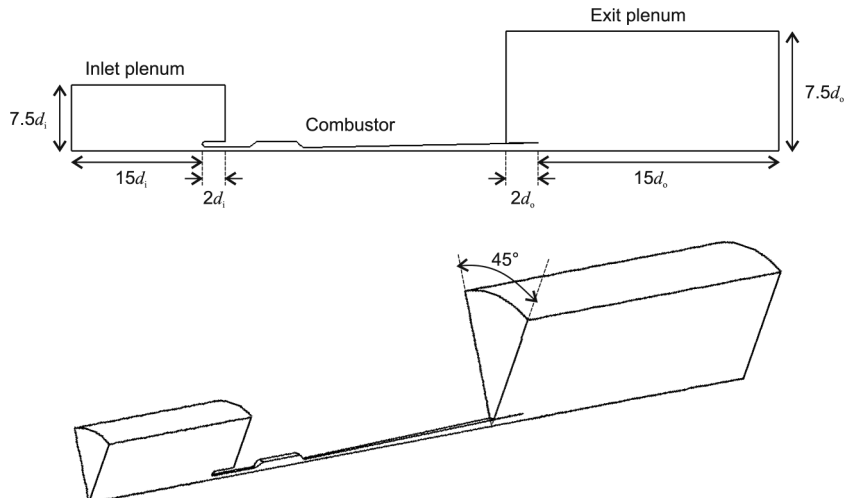

Fig. 5   Schematic of the computational domain (d_i = inlet diameter, d_o = exit diameter).

steady rate of heat transfer out through the walls; however, because the combustor pressure oscillates approximately sinusoidally about the dead-state pressure, this heat transfer only has a small net effect on the creation of mechanical work potential within the combustor. The plenums at each end of the combustor allowed the ambient fluid surrounding the experimental combustor to be modeled. Nonreflecting atmospheric pressure boundaries were applied to the plenum walls. A 45 deg slice of the experimental combustor was modeled, with symmetry boundaries on the two sliced faces, to recreate the combustor's four axially symmetric fuel injection orifices.

Three mesh dependence studies were undertaken. The first was on the penetration depth of the injected fuel jet. The number of mesh points across the fuel nozzle was raised until the penetration depth of the fuel jet within the combustor became mesh independent. This was found to require ten cells across the jet diameter at the point of injection. The second study was on the vortex roll up in the combustion chamber. This mechanism is the key driver of heat release [9]. The mesh resolution in the combustor was increased until the heat release per cycle became independent of mesh resolution. This required 1 million cells in the combustor. The final study was on the pressure wave in the inlet and tail pipe. The axial number of mesh points in the inlet and tail pipe was increased until the amplitude and shape of the standing wave in the combustor became independent of mesh resolution. This resulted in 1500 mesh points across the wavelength of the fundamental mode of the combustor. The total number of mesh points in the overall domain was 1.7 million cells.

The simulation was set up to produce transient, turbulent, reacting solutions. A timestep of 0.5 μs was used, which resulted in approximately 10,000 timesteps per combustor cycle ($\sim$5 ms). The gases were modeled as semiperfect, with specific heat capacities for each species calculated from empirical polynomial functions of temperature. Combustion was simulated using the Weller 3-equation model. Turbulence was simulation using the k-ε renormalization group model. Use of the more sophisticated RSM Speziale–Sarkar–Gatski model was found to have a negligible effect on the predicted amplitude of the acoustic standing wave.

C.   Validation of Simulation

To validate the performance of the simulated combustor, the predicted thrust-specific fuel consumption (SFC) was compared with experimental measurements. SFC is defined as the fuel massflow rate, divided by the sum of the time-averaged thrust magnitudes measured at the inlet pipe and tailpipe. The comparison of predicted and measured SFCs is shown in Fig. 6. It can be seen that there is good agreement between simulation and experiment across the whole range of fuel massflow rates.

To validate the strength and structure of the waves within the simulated combustor, the predicted time-resolved pressures at four fuel massflow rates were compared with experimental measurements. This comparison is shown in Fig. 7. Good agreement can be seen across the first three fuel massflow rates shown. At the highest fuel massflow rate, the experimental pressure trace can be seen to be more "peaky" than the predicted trace. This indicates that, at this fuel

flow rate, shocks are starting to form, which are not captured by the simulation.

The accuracy of the simulation in predicting the operation of the experimental combustor is surprising. It is thought that the reason for this is that, in valveless pulse combustors, the heat release is largely controlled by a single large-scale vortical roll up within the combustion chamber. Provided this roll-up mechanism is correctly resolved, the heat release mechanism will be accurately predicted. This is in agreement with the findings of Offord et al. [9]. Future large-eddy simulations of a pulse combustor would be of use in validating this hypothesis.

D.   Rayleigh Efficiency

The computationally predicted Rayleigh efficiency of the pulse combustor is plotted against fuel massflow rate in Fig. 8. It can be seen from the figure that Rayleigh efficiency rises as fuel massflow rate is increased, all the way to the highest flow rate of 3.35 g/s. This is unlike the SFC of the combustor, which is minimized at roughly 1.8 g/s. This finding challenges the commonly held view that SFC is an appropriate performance metric to use with pressure gain combustors for gas turbine applications [10]. The rise in Rayleigh efficiency with fuel massflow rate can be explained by the fact that the amplitude of the pressure wave within the combustor increases as fuel flow rate is increased. The average pressure at which heat release occurs therefore rises, resulting in a more efficient conversion of heat to mechanical work potential.

The computationally predicted fluxes of mechanical work potential leaving the combustor are plotted against fuel massflow rate in Fig. 9. The split of mechanical work potential between the inlet pipe and tailpipe jets can be seen. The tailpipe jet carries roughly 60% more mechanical work potential than the inlet pipe jet.

The combustor's peak Rayleigh efficiency of 3.8% can be compared with the Rayleigh efficiencies of other published pulse combustors. Five measurements of pressure gain have been reported in the literature [8,11–14]. For all five of these cases the combustor inlet and exit flows are steady, and the combustor temperature ratios are quoted. This allows the specific mechanical work potential at inlet and outlet and the specific heat input to be calculated for each case. From these calculations the Rayleigh efficiency of each combustor can be determined.

Figure 10 shows the comparison between the combustor tested in this work and the five published combustors. Historically, the combustor's outflow had to be steady to measure pressure gain, and so bypass ducts and ejectors were included in each published setup. Using the analysis method reported in this paper, the pressure gain and Rayleigh efficiency can be determined for combustors with unsteady inlet and outlet flow. As expected, due to the lack of a bypass duct, the combustor of this work has the highest Rayleigh efficiency. When comparing Kentfield et al.'s [8] combustor with that of the current study, it is interesting to note that Kentfield et al.'s combustor has a Rayleigh efficiency that is 65% of that measured in the current study. The optimal transfer efficiency of unsteady ejectors (similar to those used by Kentfield) reported in the literature is 65% [15].

E.   Mechanisms Responsible for Rayleigh Efficiency

The mechanical work potential balance equation [Eq. (12)] can be used to relate the Rayleigh efficiency of the pulse combustor to production and destruction source terms within the pulse combustor. The values of the production and destruction terms have been calculated from the results of the simulation.

It should be noted that expressing the Rayleigh efficiency in the form of Eq. (12) is only strictly true for a mixture of perfect gases, because the perfect gas assumption is invoked in the derivation of the equation. The assumption of perfect gas behavior for the purposes of mechanical work potential analysis can be justified in this work by the fact that pressures within the combustor do not exceed twice the dead-state pressure. This corresponds to a temperature ratio of approximately 1.2. Over this temperature ratio, variations in γ and c_p for each species are small. Equation (12) could have been derived for a
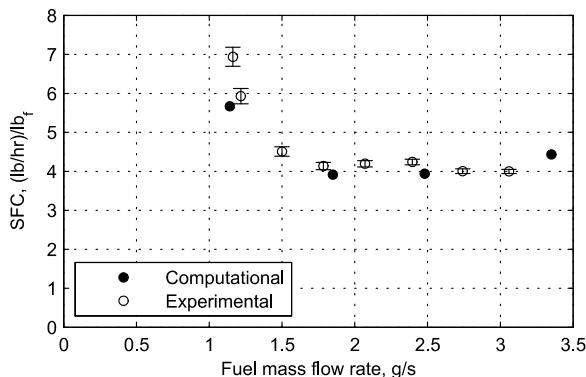

Fig. 6   Comparison of predicted and measured time-averaged SFC, with experimental error bars, plotted against fuel massflow rate.
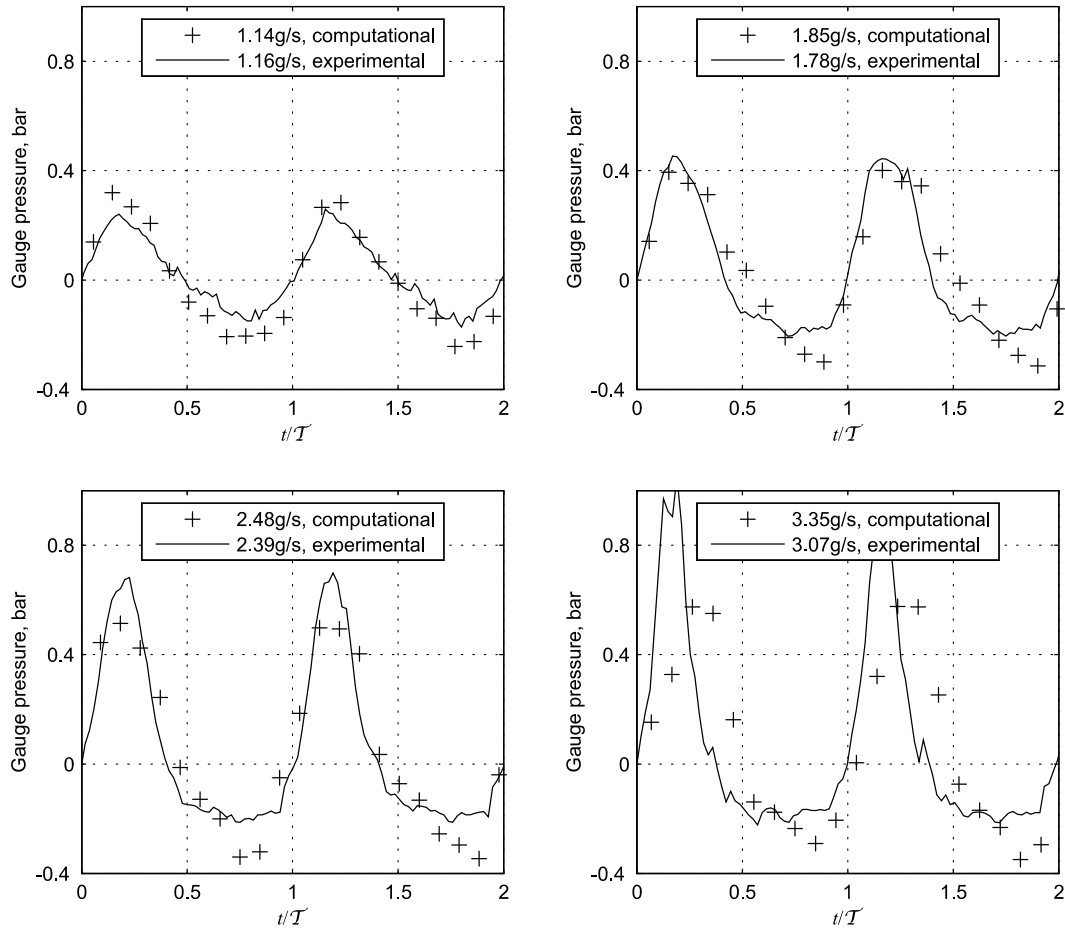
Fig. 7   Comparison of predicted and measured pressure signals from the inlet pipe at four fuel massflow rates.

mixture of semiperfect gases, but there would have been little gain in accuracy and the form of the equation would have been less clear.

All terms on the right side of Eq. (12) were calculated, but only two were found to be significant. All other terms were found to be less than 1% of their size. The significant terms were $\dot{M}_{Qr}$, representing the creation of mechanical work potential by heat release, and $\dot{M}_{\Phi}$, representing the destruction of mechanical work potential by viscous dissipation. Setting the small terms to zero allows Eq. (12) to be rewritten as

$$\eta_R = \frac{\frac{1}{\mathcal{T}} \int_{\mathcal{T}} (\dot{M}_{Qr} - \dot{M}_{\Phi})\, dt}{\dot{Q}} \qquad (13)$$

This equation shows that the combustor's Rayleigh efficiency is equal to the time-averaged rate of creation of mechanical work potential by heat release, minus the time-averaged rate of destruction
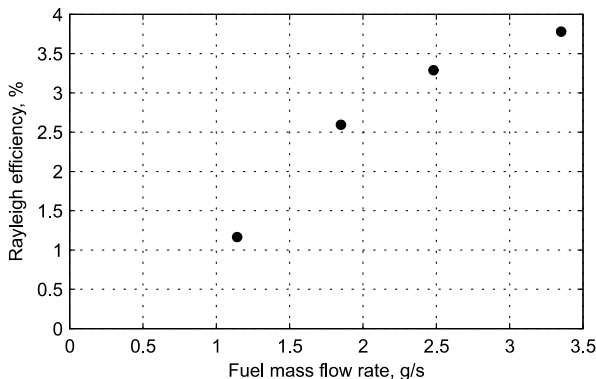
of mechanical work potential by viscous dissipation, divided by the heat input rate to the combustor.

Figure 11 shows the two source terms from Eq. (13) plotted against fuel massflow rate. It can be seen that viscous dissipation only destroys about 20% of the mechanical work potential created by heat release. This implies that viscous dissipation is not a significant factor limiting the performance of the pulse combustor.

IV.   Cycle Analysis of a Valveless Pulse Combustion Gas Turbine

The new control volume analysis is particularly useful in analyzing the impact of introducing pressure gain combustors into gas turbine cycles. In this section, a relationship between the Rayleigh efficiency of the pressure gain combustor and the thermal efficiency of a gas turbine with the pressure gain combustor installed is determined. This
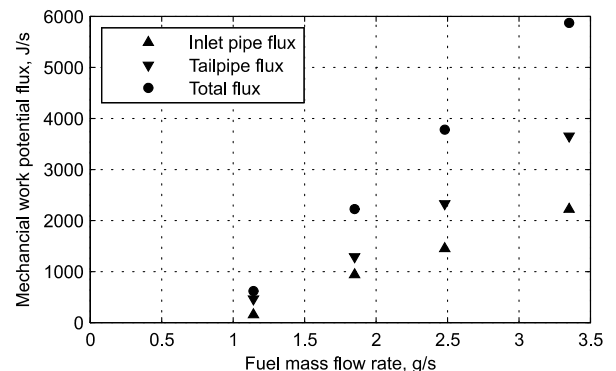

Fig. 8   Predicted Rayleigh efficiency of the pulse combustor relative to fuel massflow rate.

Fig. 9   Predicted time-averaged fluxes of mechanical work potential leaving the combustor over one cycle relative to fuel massflow rate.
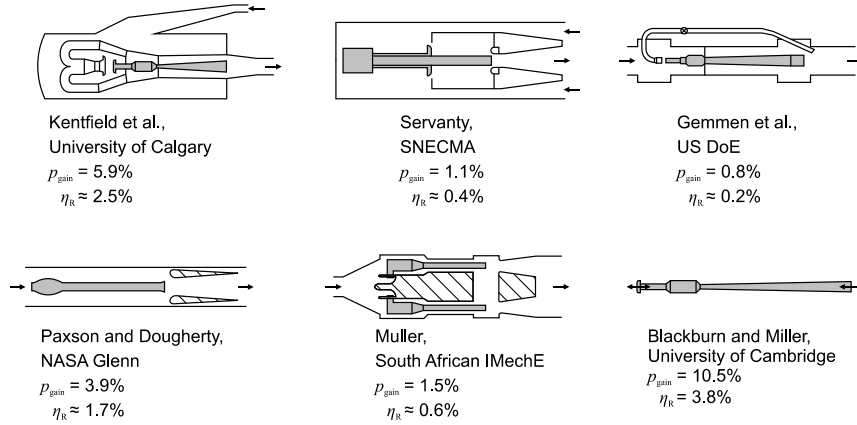
Fig. 10   Estimated Rayleigh efficiencies achieved by other researchers [8,11–14] and the Rayleigh efficiency predicted in this work.
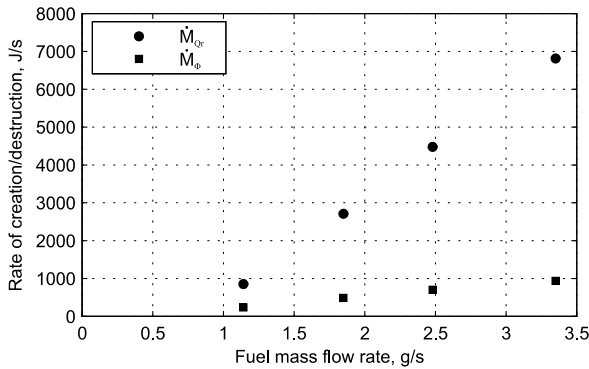

Fig. 11   Predicted time-averaged rates of creation and destruction of mechanical work potential within the pulse combustor control volume relative to fuel massflow rate.

will then be used to analyze the case study of a valveless pulse combustor presented in Sec. III.

A.   Relationship Between Thermal Efficiency and Rayleigh Efficiency

A pressure gain combustor installed in a gas turbine is shown in Fig. 12. Three control volumes are defined: control volume A, which includes the combustor; control volume B, which includes the combustor and ejector; and control volume C, which includes the whole cycle.

First, consider control volume A. The Rayleigh efficiency of this control volume is given by

$$\eta_{R,A(D2)} = \frac{\frac{1}{\mathcal{T}} \int_{\mathcal{T}} ([\dot{M}_{Qr(D2)}]_{PGC} - [\dot{M}_{\Phi(D2)}]_{PGC}) \, dt}{\dot{Q}} \qquad (14)$$

in which the subscript $D2$ indicates that the dead-state pressure for control volume A has been set equal to the compressor delivery pressure p_2.

Next, consider control volume B. The dead state of control volume B is the same as for control volume A. The Rayleigh efficiency of this control volume is therefore given by

$$\eta_{R,B(D2)} = \eta_{R,A(D2)} - \left(\frac{[\dot{M}_{\Phi(D2)}]_{\text{ejector}}}{\dot{Q}}\right) \qquad (15)$$

in which $[\dot{M}_{\Phi(D2)}]_{\text{ejector}}$ represents the rate of destruction of mechanical work potential by viscous dissipation within the ejector.

Finally, consider control volume C. The dead-state pressure of this control volume is taken to be the environmental pressure p_1. Switching the dead states changes $\dot{M}_{Qr}$ (the rate of creation of mechanical work potential by heat release) and $\dot{M}_{\Phi}$ (the rate of destruction of mechanical work potential by viscous dissipation). The change in $\dot{M}_{Qr}$ is given by

$$\dot{M}_{Qr(D1)} = \left(\frac{p_{D1}}{p_{D2}}\right)^{\frac{\gamma-1}{\gamma}} \dot{M}_{Qr(D2)} + \left[1 - \left(\frac{p_{D1}}{p_{D2}}\right)^{\frac{\gamma-1}{\gamma}}\right] \dot{Q} \qquad (16)$$

Changing the dead state has two effects. The first term shows that $\dot{M}_{Qr}$ is scaled by a reheat factor set by the ratio of the two dead-state pressures. The second term is a Brayton cycle thermal efficiency between the two dead states.

The change in $\dot{M}_{\Phi}$ is given by

$$\dot{M}_{\Phi(D1)} = \left(\frac{p_{D1}}{p_{D2}}\right)^{\frac{\gamma-1}{\gamma}} \dot{M}_{\Phi(D2)} \qquad (17)$$

Changing the dead state can be seen to simply scale $\dot{M}_{\Phi}$ by a reheat factor set by the ratio of the two dead-state pressures. The effect of changing dead-state pressures in this analysis is analogous to the effect of changing dead states in an exergy analysis. The only difference is that, in this analysis, the reheat factor is $(p_{D1}/p_{D2})^{\frac{\gamma-1}{\gamma}}$ rather than T_{D1}/T_{D2}.
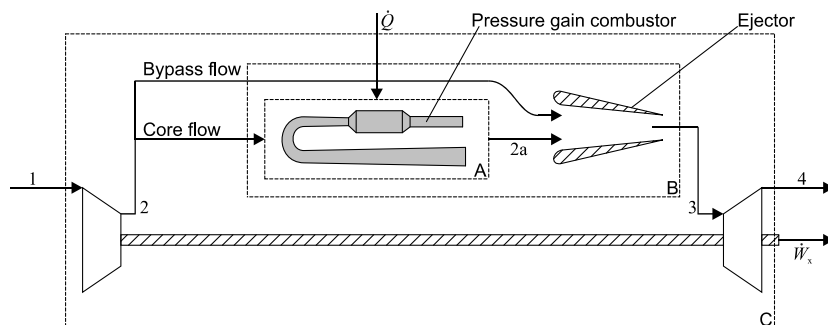

Fig. 12   Integration of a valveless pulse combustor within a gas turbine, showing pressure gain combustor control volume (A), combustor and ejector control volume (B), and gas turbine control volume (C).

The Rayleigh efficiency of control volume C can now be written as

$$
\eta_{R,C(D1)} = \left(\frac{p_{D1}}{p_{D2}}\right)^{\frac{\gamma-1}{\gamma}} \left[\overbrace{\left(\frac{\frac{1}{T}\int_T ([\dot{M}_{Qr(D2)}]_{PGC} - [\dot{M}_{\Phi(D2)}]_{PGC})\,dt}{\dot{Q}}\right)}^{=\eta_{R,A(D2)}} \right.
$$
$$
\left. - \left(\frac{[\dot{M}_{\Phi(D2)}]_{ejector}}{\dot{Q}}\right) \right] + \left[1 - \left(\frac{p_{D1}}{p_{D2}}\right)^{\frac{\gamma-1}{\gamma}}\right] - \left[\frac{[\dot{M}_{\Phi(D1)}]_{turbomachinery}}{\dot{Q}}\right]
\tag{18}
$$

Equation (18) can be rewritten as

$$
\eta_{R,C(D1)} = \left(\frac{p_{D1}}{p_{D2}}\right)^{\frac{\gamma-1}{\gamma}} \eta_{R,A(D2)} + \left[1 - \left(\frac{p_{D1}}{p_{D2}}\right)^{\frac{\gamma-1}{\gamma}}\right]
$$
$$
- \left(\frac{[\dot{M}_{\Phi(D1)}]_{turbomachinery} + [\dot{M}_{\Phi(D1)}]_{ejector}}{\dot{Q}}\right)
\tag{19}
$$

If the kinetic energy at inlet and exit of control volume C is zero, then the Rayleigh efficiency and thermal efficiency of the control volume can be directly related:

$$
\eta_{R,C(D1)} = \frac{w_x + \overbrace{m_{f,4}}^{=0} - \overbrace{m_{f,1}}^{=0}}{c_p(T_{0,3} - T_{0,2})} = \eta_{th,C}
\tag{20}
$$

Substituting Eq. (19) into Eq. (20) gives the relationship between the thermal efficiency of the cycle and the Rayleigh efficiency of the combustor:

$$
\eta_{th,C} = \overbrace{\left(\frac{p_{D1}}{p_{D2}}\right)^{\frac{\gamma-1}{\gamma}} \eta_{R,A(D2)}}^{\text{Pulse combustor Rayleigh efficiency relative to dead-state 1}} + \overbrace{\left[1 + \left(\frac{p_{D1}}{p_{D2}}\right)^{\frac{\gamma-1}{\gamma}}\right]}^{\text{Brayton cycle thermal efficiency between the two dead states}}
$$
$$
- \overbrace{\left[\frac{[\dot{M}_{\Phi(D1)}]_{ejector} + [\dot{M}_{\Phi(D1)}]_{turbomachinery}}{\dot{Q}}\right]}^{\text{Viscous destruction of mechanical work potential in ejector and turbomachinery relative to dead-state 1}}
\tag{21}
$$

Equation (21) shows that the effect on its thermal efficiency of introducing a pressure gain combustor into a gas turbine cycle can simply be determined by scaling the combustor's Rayleigh efficiency by a reheat factor, based on the two dead-state pressures, and adding it to the thermal efficiency of the baseline gas turbine.

B. Cycle Thermal Efficiency

In this section, the valveless pulse combustor reported in Sec. III is introduced into a gas turbine. The cycle analysis developed in the preceding section is used to determine the performance improvement. A schematic of the gas turbine incorporating the pulse combustor is shown in Fig. 12. The parameters of the considered gas turbine cycle are given in Table 1. A range of temperature ratios and overall compressor pressure ratios are considered in order that the thermal efficiency achieved by gas turbines of various sizes can be assessed. For simplicity, 1) the turbomachinery components are given constant isentropic efficiencies, whose values are chosen to be representative of a typical modern gas turbine, and 2) the ejector used to mix bypass flow and core flow is assumed to have zero viscous dissipation. The incoming flow to the cycle is assumed to have the properties of the international standard atmosphere at sea level. The working fluid is treated as a perfect gas with the properties of atmospheric air. The massflow rate of the cycle is treated as constant throughout, and the effects of turbine cooling flows are ignored. This cycle model is appropriate for either a power generation gas turbine or

Table 1   Gas turbine cycle parameters

Cycle parameter	Value
Overall compressor pressure ratio	1–50
Temperature ratio, $T_{0,3}/T_{0,2}$	2–3
Compressor isentropic efficiency	0.9
Turbine isentropic efficiency	0.9

an aeroengine with no forward motion. In the latter case, the cycle's work output would be used to spin a fan for propulsion.

Figure 13 shows the increase in thermal efficiency of the gas turbine when the conventional steady-flow combustor with 5% stagnation pressure loss is replaced with the pulse combustor used in this study. The figure shows that, between pressure ratios of 20 and 40 (typical for modern gas turbines), the effect of replacing a gas turbine's conventional combustor with a current design of SNECMA/Lockwood-type valveless pulse combustor would result in an increase in thermal efficiency of 2–2.5 percentage points.

For comparison purposes, a second, idealized combustor is considered. This combustor is an ideal constant-volume stoichiometric combustor. Fuel is added to the combustor inlet to form a stoichiometric mix. Combustion then occurs at constant volume. Work is then extracted from the flow to exhaust the higher-pressure fluid from the combustion chamber. It should be noted that, though idealized, this combustion process is not the optimal combustion process, because some pressure gain combustors precompress the reactants before combustion, which further raises the combustor's performance. Figure 14 shows the increase in thermal efficiency of the gas turbine when the conventional steady-flow combustor is replaced with this ideal constant-volume stoichiometric combustor. The figure shows that, between pressure ratios of 20 and 40, the effect of replacing a gas turbine's conventional combustor with an ideal constant-volume stoichiometric combustor would result in an increase in thermal efficiency of 9–12 percentage points.
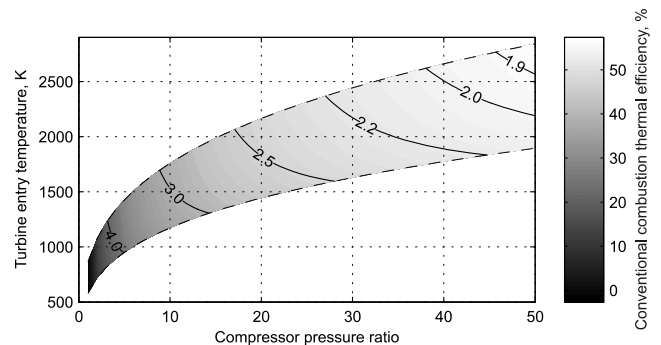

Fig. 13   The estimated thermal efficiency increase (percentage points) when the pulse combustor replaces a conventional combustor in a modern gas turbine.
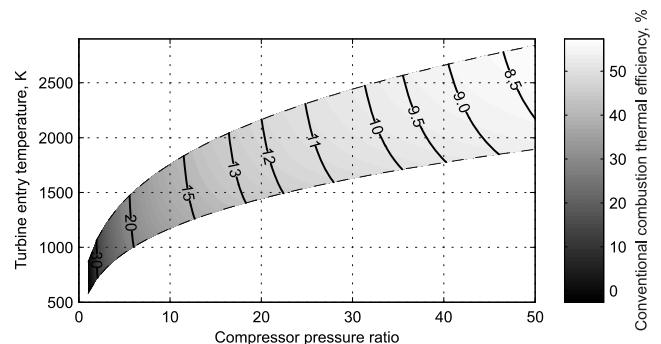

Fig. 14   The estimated thermal efficiency increase (percentage points) when an ideal constant-volume combustor replaces a conventional combustor in a modern gas turbine.

V. Conclusions

For pressure gain combustors that are for use in gas turbine applications, Rayleigh efficiency has been shown to be an effective, and easy to apply, definition of performance. It has the advantage that it can be applied to any type of pressure gain combustor and that, when applied to a gas turbine cycle, it translates easily into thermal efficiency. A pressure gain combustor therefore has two possible performance metrics: thrust-specific fuel consumption and Rayleigh efficiency. The choice of metric should be made according to the intended application of the combustor.

A control volume method that was recently developed for use in gas turbines has been extended for use with pressure gain combustors. The method directly links the performance of the combustor to the two primary source terms inside the combustor: the thermal creation term (a nonlinear analog of Lord Rayleigh's acoustic thermal energy creation term) and the viscous destruction term.

The new analysis method has been used to solve a number of unanswered questions: 1) The peak Rayleigh efficiency of a SNECMA/Lockwood-type valveless pulse combustor was shown to be 3.8%. 2) The peak efficiency does not occur at the same fuel input as the minimum specific fuel consumption. 3) The efficiency is not significantly limited by viscous dissipation within the combustor. The dissipation term is only 20% of the size of the thermal creation term. Raising efficiency therefore requires the thermal creation term to be raised.

The effect on overall gas turbine thermal efficiency, when the conventional steady-flow combustor is replaced with a valveless pulse combustor, has been determined. Between a pressure ratio of 20 and 40, typical for modern gas turbines, the effect of replacing a gas turbine's conventional combustor with a current design of SNECMA/ Lockwood-type valveless pulse combustor would result in an increase in thermal efficiency of 2–2.5 percentage points. This contrasts with an ideal constant-volume combustor, which would result in an increase in thermal efficiency of 9–12 percentage points. It should be noted that this idealized constant-volume combustor does not achieve the theoretical maximum increase in efficiency. This is because some pressure gain combustors also involve an internal precompression process.

The analysis method outlined in the paper offers the possibility of analyzing other types of combustor. The method would be especially effective for use in devices such as rotating detonation combustors in which the thermal creation terms and viscous destruction terms are much larger than in a pulse combustor and for devices for which the overall performance is determined by the difference between the two terms. The analysis method would also be a useful tool in guiding pressure gain combustor design. Regions of high viscous destruction could be targeted for streamlining, and regions of high thermal creation could be targeted to increase rates of heat release.

Appendix A: Derivation of the Mechanical Work Potential Balance Equation

In this appendix, the mechanical work potential balance equation is derived for a nonuniform mixture of perfect gases. First, the balance equation is derived in differential form, then the differential form is used to derive the balance equation in integral form. To begin, expressions are needed for the specific system mechanical work potential and the specific flow mechanical work potential. Miller [5] showed that these quantities can be written as

$$\mathsf{m} = c_v T\left(1 - \frac{T_{se}}{T}\right) + p_D(v - v_{se}) + \frac{|U|^2}{2} \tag{A1}$$

$$\mathsf{m}_f = \mathsf{m} + (p - p_D)v = c_p T\left(1 - \frac{T_{se}}{T}\right) + \frac{|U|^2}{2} \tag{A2}$$

A1   Mechanical Work Potential Balance in Differential Form

The material derivative of the system specific mechanical work potential, written in what is referred to as the divergence or field form, is

$$\rho\frac{\mathrm{D}\mathsf{m}}{\mathrm{D}t} = \rho\frac{\partial \mathsf{m}}{\partial t} + \rho U \cdot \nabla \mathsf{m} = \frac{\partial \rho \mathsf{m}}{\partial t} + \nabla \cdot (\rho U \mathsf{m}) \tag{A3}$$

Using this equation and general vector identities, the local-time rate of change and the advection rate of change of system mechanical work potential can be written separately as

$$\frac{\partial \rho \mathsf{m}}{\partial t} = \left(1 - \frac{T_{se}}{T}\right)\frac{\partial \rho c_v T}{\partial t} + \rho c_v T\frac{\partial}{\partial t}\left(1 - \frac{T_{se}}{T}\right)$$
$$+ p_D\frac{\partial \rho(v - v_{se})}{\partial t} + \frac{\partial}{\partial t}\left(\rho\frac{|U|^2}{2}\right) \tag{A4}$$

$$\nabla \cdot (\rho U \mathsf{m}) = \left(1 - \frac{T_{se}}{T}\right)\nabla \cdot (\rho U c_v T) + (\rho U c_v T)\cdot\nabla\left(1 - \frac{T_{se}}{T}\right)$$
$$+ \nabla \cdot [\rho U p_D(v - v_{se})] + \nabla \cdot \left(\rho U\frac{|U|^2}{2}\right) \tag{A5}$$

The third term on the right side of Eq. (A5) can be expanded to give

$$\nabla \cdot [\rho U p_D(v - v_{se})] = \nabla \cdot (p_D U) - p_D\frac{v_{se}}{v}\nabla \cdot U - (p_D U)\cdot\nabla\left(\frac{v_{se}}{v}\right) \tag{A6}$$

Substituting Eqs. (A4–A6) into Eq. (A3) gives the following expression for the material derivative of the specific system mechanical work potential:

$$\frac{\partial \rho \mathsf{m}}{\partial t} + \nabla \cdot (\rho U \mathsf{m}) = \left(1 - \frac{T_{se}}{T}\right)\left[\frac{\partial \rho c_v T}{\partial t} + \nabla \cdot (\rho U c_v T)\right]$$
$$+ \left[\frac{\partial}{\partial t}\left(\rho\frac{|U|^2}{2}\right) + \nabla \cdot \left(\rho U\frac{|U|^2}{2}\right)\right]$$
$$+ \nabla \cdot (p_D U) - p_D\frac{v_{se}}{v}\nabla \cdot U - \rho c_v T\frac{\mathrm{D}}{\mathrm{D}t}\left(\frac{T_{se}}{T}\right) - p_D\frac{\mathrm{D}}{\mathrm{D}t}\left(\frac{v_{se}}{v}\right) \tag{A7}$$

The first two terms on the right side of Eq. (A7) contain the material derivatives of the internal and kinetic energy. The conservation equations for internal (thermal) and kinetic energy in differential form are given by [16]

$$\left[\frac{\partial \rho c_v T}{\partial t} + \nabla \cdot (\rho U c_v T)\right] = -\nabla \cdot \boldsymbol{q} + \dot{q} - p(\nabla \cdot U) + \Phi \tag{A8}$$

$$\left[\frac{\partial}{\partial t}\left(\rho\frac{|U|^2}{2}\right) + \nabla \cdot \left(\rho U\frac{|U|^2}{2}\right)\right]$$
$$= \nabla \cdot (\bar{\bar{\tau}} \cdot U) - [\nabla \cdot (pU) - p(\nabla \cdot U)] - \Phi \tag{A9}$$

Substituting Eqs. (A8) and (A9) into Eq. (A7) gives

$$\frac{\partial \rho \mathsf{m}}{\partial t} + \nabla \cdot (\rho U \mathsf{m}) = \left(1 - \frac{T_{se}}{T}\right)(-\nabla \cdot \boldsymbol{q} + \dot{q}) + \nabla \cdot (\bar{\bar{\tau}} \cdot U) - \frac{T}{T_{se}}\Phi$$
$$- \nabla \cdot [U(p - p_D)] - \rho c_v T\frac{\mathrm{D}}{\mathrm{D}t}\left(\frac{T_{se}}{T}\right) - p_D\frac{\mathrm{D}}{\mathrm{D}t}\left(\frac{T_{se}}{T}\right) \tag{A10}$$

Moving the fourth term on the right side of Eq. (A10) to the left side gives the final version of the conservation equation for mechanical work potential in differential form:

$$\frac{\partial \rho \mathsf{m}}{\partial t} + \nabla \cdot (\rho U \mathsf{m}_f) = \left(1 - \frac{T_{se}}{T}\right)(-\nabla \cdot \boldsymbol{q} + \dot{q}) + \nabla \cdot (\bar{\bar{\tau}} \cdot U)$$

$$- \frac{T}{T_{se}}\Phi - \rho c_v T \frac{\mathrm{D}}{\mathrm{D}t}\left(\frac{T_{se}}{T}\right) - p_D \frac{\mathrm{D}}{\mathrm{D}t}\left(\frac{v_{se}}{v}\right) \qquad (A11)$$

A2 Mechanical Work Potential Balance in Integral Form

An integral expression for the conservation of mechanical work potential can be derived by integrating Eq. (A11) over a general control volume V. Applying Reynolds' transport theorem, to account for the time dependence of the specific system mechanical work potential and the dynamic boundaries of the control volume, gives the following expression for the rate of change of mechanical work potential in the volume:

$$\frac{\mathrm{d}}{\mathrm{d}t}\iiint_V \rho \mathsf{m}\,\mathrm{d}V - \oiint \rho \mathsf{m} S \cdot \hat{\boldsymbol{n}}\,\mathrm{d}S + \oiint \rho \mathsf{m}_f U \cdot \hat{\boldsymbol{n}}\,\mathrm{d}S$$

$$= \iiint_V \left[\left(1 - \frac{T_{se}}{T}\right)(-\nabla \cdot \boldsymbol{q} + \dot{q}) + \nabla \cdot (\bar{\bar{\tau}} \cdot U)\right.$$

$$\left. - \frac{T}{T_{se}}\Phi - \rho c_v T \frac{\mathrm{D}}{\mathrm{D}t}\left(\frac{T_{se}}{T}\right) - p_D \frac{\mathrm{D}}{\mathrm{D}t}\left(\frac{v_{se}}{v}\right)\right]\mathrm{d}V \qquad (A12)$$

The control volume surface can be split into three types of sub-surfaces: fixed walls S_{FW} (such that $(U \cdot \hat{\boldsymbol{n}} = 0)$); moving walls S_{MW} (such that $(U \cdot \hat{\boldsymbol{n}} = S \cdot \hat{\boldsymbol{n}})$); and input/output boundaries S_{IO}. After splitting the second and third terms on the left side of Eq. (A12) into subsurface integrals, the mechanical work potential balance in integral form can be written as

$$\frac{\mathrm{d}}{\mathrm{d}t}\iiint_V \rho \mathsf{m}\,\mathrm{d}V + \iint_{S_{\mathrm{IO}}} \rho \mathsf{m}_f U \cdot \hat{\boldsymbol{n}}\,\mathrm{d}S + \iint_{S_{\mathrm{MW}}} (p - p_D) S \cdot \hat{\boldsymbol{n}}\,\mathrm{d}S$$

$$= \iiint_V \left[\left(1 - \frac{T_{se}}{T}\right)(-\nabla \cdot \boldsymbol{q} + \dot{q}) + \nabla \cdot (\bar{\bar{\tau}} \cdot U)\right.$$

$$\left. - \frac{T}{T_{se}}\Phi - \rho c_v T \frac{\mathrm{D}}{\mathrm{D}t}\left(\frac{T_{se}}{T}\right) - p_D \frac{\mathrm{D}}{\mathrm{D}t}\left(\frac{T_{se}}{T}\right)\right]\mathrm{d}V \qquad (A13)$$

The heat flux term on the right side of Eq. (A13) can be split into two parts, representing the effects of heat transfer across the control volume surface and internal heat transfer within the control volume:

$$\left(1 - \frac{T_{se}}{T}\right)\nabla \cdot \boldsymbol{q} = \nabla \cdot \left[\left(1 - \frac{T_{se}}{T}\right)\boldsymbol{q}\right] + \boldsymbol{q} \cdot \nabla \left(\frac{T_{se}}{T}\right) \qquad (A14)$$

Equation (A14) can be substituted back into Eq. (A13), and the moving wall sub-surface integral can be moved to the right side. Applying Gauss' theorem and using the isentropic relationships for perfect gases yields the following balance equation for mechanical work potential:

$$\frac{\mathrm{d}}{\mathrm{d}t}\iiint_V \rho \mathsf{m}\mathrm{d}V + \iint_{S_{\mathrm{IO}}} \rho \mathsf{m}_f U \cdot \hat{n}\,\mathrm{d}S = -\iint_{S_{\mathrm{MW}}}[(p - p_D)S \cdot \hat{n} - \boldsymbol{\tau} \cdot S]\mathrm{d}S$$

$$+ \oiint \left(1 - \left(\frac{p_D}{p}\right)^{\frac{\gamma-1}{\gamma}}\right)(-\boldsymbol{q}) \cdot \hat{n}\,\mathrm{d}S + \iiint_V \left(1 - \left(\frac{p_D}{p}\right)^{\frac{\gamma-1}{\gamma}}\right)\dot{q}\,\mathrm{d}V$$

$$- \iiint_V \boldsymbol{q} \cdot \nabla \left[\left(\frac{p_D}{p}\right)^{\frac{\gamma-1}{\gamma}}\right]\mathrm{d}V - \iiint_V \left(\frac{p_D}{p}\right)^{\frac{\gamma-1}{\gamma}}\Phi\,\mathrm{d}V$$

$$- \iiint_V \rho c_v T \frac{\mathrm{D}}{\mathrm{D}t}\left[\left(\frac{p_D}{p}\right)^{\frac{\gamma-1}{\gamma}}\right]\mathrm{d}V - \iiint_V p_D \frac{\mathrm{D}}{\mathrm{D}t}\left[\left(\frac{p_D}{p}\right)^{\frac{-1}{\gamma}}\right]\mathrm{d}V \qquad (A15)$$

The fourth term on the right side of Eq. (A15), which represents the effect of internal heat transfer, can be split into two terms. The first of these terms represents the effect of heat transfer across an internal pressure gradient, whereas the second represents the effect of heat transfer across an internal gas composition gradient:

$$-\boldsymbol{q} \cdot \nabla \left[\left(\frac{p_D}{p}\right)^{\frac{\gamma-1}{\gamma}}\right] = \left(\frac{\gamma-1}{\gamma}\right)\left(\frac{p_D}{p}\right)^{\frac{\gamma-1}{\gamma}}\frac{\nabla p}{p} \cdot \boldsymbol{q}$$

$$+ \left(\frac{p_D}{p}\right)^{\frac{\gamma-1}{\gamma}}\ln\left[\left(\frac{p_D}{p}\right)^{\frac{-1}{\gamma}}\right]\frac{\nabla \gamma}{\gamma} \cdot \boldsymbol{q} \qquad (A16)$$

The sixth and seventh terms on the right side of Eq. (A15) can be manipulated to yield a single term representing the effect of internal molecular diffusion changing the composition of material elements:

$$-\rho c_v T \frac{\mathrm{D}}{\mathrm{D}t}\left[\left(\frac{p_D}{p}\right)^{\frac{\gamma-1}{\gamma}}\right] - p_D \frac{\mathrm{D}}{\mathrm{D}t}\left[\left(\frac{p_D}{p}\right)^{\frac{-1}{\gamma}}\right]$$

$$= \left(\frac{p_D}{p}\right)^{\frac{\gamma-1}{\gamma}}\ln\left[\left(\frac{p_D}{p}\right)^{\frac{-1}{\gamma}}\right]\frac{1}{\gamma}\frac{\mathrm{D}\gamma}{\mathrm{D}t}\rho c_p T \qquad (A17)$$

Substituting Eqs. (A16) and (A17) back into Eq. (A15) gives the final form of the mechanical work potential balance equation in integral form:

$$\frac{\mathrm{d}}{\mathrm{d}t}\iiint_V \rho \mathsf{m}\,\mathrm{d}V + \iint_{S_{\mathrm{IO}}} \rho \mathsf{m}_f U \cdot \hat{\boldsymbol{n}}\,\mathrm{d}S = -\iint_{S_{\mathrm{MW}}}[(p - p_D)S \cdot \hat{\boldsymbol{n}} - \boldsymbol{\tau} \cdot S]\mathrm{d}S$$

$$+ \oiint \left(1 - \left(\frac{p_D}{p}\right)^{\frac{\gamma-1}{\gamma}}\right)(-\boldsymbol{q}) \cdot \hat{\boldsymbol{n}}\,\mathrm{d}S + \iiint_V \left(1 - \left(\frac{p_D}{p}\right)^{\frac{\gamma-1}{\gamma}}\right)\dot{q}\,\mathrm{d}V$$

$$+ \iiint_V \left(\frac{p_D}{p}\right)^{\frac{\gamma-1}{\gamma}}\left(\frac{\gamma-1}{\gamma}\right)\frac{\nabla p}{p} \cdot \boldsymbol{q}\,\mathrm{d}V$$

$$+ \iiint_V \left(\frac{p_D}{p}\right)^{\frac{\gamma-1}{\gamma}}\ln\left[\left(\frac{p_D}{p}\right)^{\frac{-1}{\gamma}}\right]\frac{\nabla \gamma}{\gamma} \cdot \boldsymbol{q}\,\mathrm{d}V$$

$$- \iiint_V \left(\frac{p_D}{p}\right)^{\frac{\gamma-1}{\gamma}}\Phi\,\mathrm{d}V + \iiint_V \left(\frac{p_D}{p}\right)^{\frac{\gamma-1}{\gamma}}\ln\left[\left(\frac{p_D}{p}\right)^{\frac{-1}{\gamma}}\right]\frac{1}{\gamma}\frac{\mathrm{D}\gamma}{\mathrm{D}t}\rho c_p T\,\mathrm{d}V$$

$$(A18)$$

References

[1] Lockwood, R. M., and Patterson, W. G., "Summary Report on Investigation of Miniature Valveless Pulsejets," Hiller Aircraft Co., Advanced Research Division, Tech. Rept. ARD-307, Palo Alto, CA, 1964.

[2] Wintenberger, E., Austin, J. M., Cooper, M., Jackson, S., and Shepherd, J. E., "Analytical Model for the Impulse of Single-Cycle Pulse Detonation Tube," *Journal of Propulsion and Power*, Vol. 19, No. 1, 2003, pp. 22–38.
doi:10.2514/2.6099

[3] Mason, S. A., Miller, R. J., and Taylor, M. D., "Fluid Mechanics of Pulsed Pressure-Gain Combustors," *46th AIAA Aerospace and Science Meeting and Exhibit*, AIAA Paper 2008-118, 2008.

[4] Rayleigh, J. W. S., "The Explanation of Certain Acoustical Phenomena," *Journal of Nature*, Vol. 18, No. 455, 1878, pp. 319–321.

[5] Miller, R. J., "Mechanical Work Potential," *ASME Turbo Expo: Turbine Technical Conference and Exposition*, American Soc. of Mechanical Engineers GT2013-95488, New York, 2013.

[6] Cumpsty, N. A., and Horlock, J. H., "Averaging Nonuniform Flow for a Purpose," *Journal of Turbomachinery*, Vol. 128, No. 1, 2006, pp. 120–129.
doi:10.1115/1.2098807

[7] Swithenbank, J., Brown, D. J., and Saunders, R. J., "The Application of Pulsating Combustion to Power Generation Using Gas Turbines," *Proceedings of the First International Symposium on Pulsed Combustion*, edited by Brown, D. J., University of Sheffield, Sheffield, U.K., 1971, pp. 10-1–10-21.

[8] Kentfield, J. A. C., Rehman, A., and Cronje, J., "Performance of Pressure-Gain Combustors Without Moving Parts," *AIAA Journal of Energy*, Vol. 4, No. 2, 1980, pp. 56–63.
doi:10.2514/3.62460

[9] Offord, T., Miller, R. J., Dawson, J. R., Heffer, J. H., Mason, S. A., and Taylor, M., "Improving the Performance of a Valveless Pulse Combustor Using Unsteady Fuel Injection," *46th AIAA Aerospace and Science Meeting and Exhibit*, AIAA Paper 2008-120, 2008.

[10] Kentfield, J. A. C., and Fernandes, L. C. V., "Improvements to the Performance of a Prototype Pulse, Pressure-Gain, Gas Turbine Combustor," *Journal of Engineering for Gas Turbines and Power*, Vol. 112, No. 1, 1990, pp. 67–72.
doi:10.1115/1.2906479

[11] Servanty, P., "Design and Testing of Harmonic Burners for Low Power Gas Turbines," *Proceedings of the First International Symposium on Pulsed Combustion*, edited by Brown, D. J., University of Sheffield, Sheffield, U.K., 1971, pp. 12-1–12-25.

[12] Gemmen, R. S., Janus, M. C., Richards, G. A., Norton, T. S., and Rogers, W. A., "Achieving Improved Cycle Efficiency via Pressure Gain Combustors," *ASME International Gas Turbine and Aeroengine Congress and Exposition*, American Soc. of Mechanical Engineers 95-GT-063, New York, 1995.

[13] Muller, J. L., "Theoretical and Practical Aspects of the Application of Resonant Combustion Chambers in Gas Turbines," *Journal of Mechanical Engineering Science*, Vol. 13, No. 3, 1971, pp. 137–150.
doi:10.1243/JMES_JOUR_1971_013_026_02

[14] Paxson, D. E., and Dougherty, K., "Ejector Enhanced Pulsejet Based Pressure Gain Combustors: An Old Idea with a New Twist," *41st AIAA/ASME/SAE/ASEE Joint Propulsion Conference and Exhibit*, AIAA Paper 2005-4216, 2005.

[15] Heffer, J. J., Miller, R. J., and Freeman, C., "Performance of Choked Unsteady Ejector-Nozzles for Use in Pressure-Gain Combustors," *46th AIAA Aerospace and Science Meeting and Exhibit*, AIAA Paper 2009-1063, 2009.

[16] Bird, R. B., "The Equations of Change and the Macroscopic Mass, Momentum, and Energy Balances," *Chemical Engineering Science*, Vol. 6, No.3, 1957, pp. 123–131.
doi:10.1016/0009-2509(57)85005-2

F. Lu
Associate Editor